CFD Analysis of Fluidic Device

Technical Report

Rev. 0

Non-Proprietary

June 2014

Revision History

Revision	Date	Page	Description
0	June 2014	All	Original Issue

ABSTRACT

The Safety Injection Tank (SIT) with Fluidic Device (FD) is an accumulator tank that is partially filled with borated water and is pressurized with nitrogen. The FD is a passive flow controller, which is installed in the bottom of the SIT, which controls the discharge flow rate in a passive manner without any moving parts. The SIT-FD design has benefits for the reactor core cooling and the inherent reliability of safety system comparing with a conventional SIT design since FD can extend duration of the SIT operation by controlling the discharge flow during reflood phase of the Large Break Loss of Coolant Accident (LBLOCA). Adoption of the FD design allows an optimization of Emergency Core Cooling System (ECCS) in the APR1400 design by elimination of Low Pressure Safety Injection Pump (LPSIP) and reduces the core damage frequency of APR1400.

The performance of the FD has been evaluated by repeated experiments in the full-scale Valve Performance Evaluation Rig (VAPER) test facility at the Korea Atomic Energy Research Institute (KAERI). Topical Report “Fluidic Device Design for the APR1400”, APR1400-Z-M-TR-12003-P, has been submitted to suggest the operation mechanism, the performance of the SIT-FD and confirmatory full scale experiments. However, detailed informations in the vortex chamber and discharge tube are not enough to understand the relationship between detailed flow characteristics in the vortex chamber and the performance of the SIT-FD, which may include cavitation phenomena.

This report provides Computational Fluid Dynamics (CFD) analysis results of the SIT-FD, which is conducted to demonstrate the full scale experiments as below.

- To confirm flow characteristics and occurrence of vaporous cavitation in the FD for both large and small flow mode.
- To predict facing angle effects by comparing the performance of the nominal design with the performance of the maximum tolerance design due to a manufacturing tolerance.

TABLE OF CONTENTS

1. INTRODUCTION 1-1

2. OBJECTIVE 2-1

3. ANALYSIS MODELS 3-2

3.1. SIT-FD Descriptions 3-2
3.2. Geometrical Modeling and Mesh Configuration 3-3
3.3. Numerical Models 3-14

4. CFD ANALYSIS 4-1

4.1. Boundary Conditions and Analysis Matrix 4-1
4.2. Sensitivity Analysis 4-5
4.3. Analysis Results 4-26

5. CONCLUSION 5-1

6. REFERENCES 6-1

LIST OF TABLES

Table 3.2-1 Total number of elements for the large flow and small flow mode……..3-7
Table 3.2-2 Mesh refinement information for the mesh sensitivity analysis……..3-8
Table 4.1-1 Summary of boundary conditions for large and small flow mode……..4-3
Table 4.2-1 Test Matrix for the advection scheme sensitivity……..4-7
Table 4.2-2 Analysis results for the advection scheme sensitivity……..4-8
Table 4.2-3 Analysis results for the mesh sensitivity analysis……..4-15
Table 4.2-4 Total number of elements and Test Matrix for the facing angle sensitivity analysis……..4-19
Table 4.2-5 Analysis results for the facing angle sensitivity analysis……4-20
Table 4.3-1 Analysis results for the large flow and small flow mode……..4-28

LIST OF FIGURES

Figure 3.2-1 Geometrical models for CFD analysis (Side-view).....3-4
Figure 3.2-2 Geometrical models for CFD analysis (Bottom-view) 3-5
Figure 3.2-3 Mesh configuration (Side-view).....3-9
Figure 3.2-4 Mesh configuration (Bottom-view).....3-10
Figure 3.2-5 Prism mesh for boundary layer.....3-11
Figure 3.2-6 Maximum Y+ for large flow case.....3-12
Figure 3.2-7 Maximum Y+ for small flow case.....3-13
Figure 4.1-1 Linear fitting data and CFD analysis points for large flow and small flow mode(Test Case-01-01) 4-4
Figure 4.2-1 Results of sensitivity analysis for selecting the advection scheme(Large flow mode, L-CASE1) 4-9
Figure 4.2-2 Results of sensitivity analysis for selecting the advection scheme(Small flow mode, S-CASE2) 4-10
Figure 4.2-3 Void fraction in the exit nozzle @ Upwind case.....4-11
Figure 4.2-4 Void fraction in the exit nozzle @ SB-[ ]TS case.....4-12
Figure 4.2-5 Void fraction in the exit nozzle @ SB-[ ]TS case.....4-13
Figure 4.2-6 Results of the mesh sensitivity analysis.....4-16
Figure 4.2-7 Comparison of the geometry models for the facing angle sensitivity analysis 4-21
Figure 4.2-8 Void fraction in the exit nozzle @ L1 case.....4-22
Figure 4.2-9 Void fraction in the exit nozzle @ L3 case.....4-23
Figure 4.2-10 Void fraction in the exit nozzle @ S1 case.....4-24
Figure 4.2-11 Void fraction in the exit nozzle @ S3 case.....4-25
Figure 4.3-1 Velocity in the vortex chamber @ L-CASE1.....4-29
Figure 4.3-2 Velocity in the vortex chamber @ L-CASE2.....4-30
Figure 4.3-3 Velocity vector in the discharge tube @ L-CASE1.....4-31
Figure 4.3-4 Velocity vector in the discharge tube @ L-CASE2.....4-32
Figure 4.3-5 Pressure distribution in the vortex chamber @ L-CASE1.....4-33
Figure 4.3-6 Pressure distribution in the vortex chamber @ L-CASE2.....4-34
Figure 4.3-7 Void fraction in the discharge tube @ L-CASE1.....4-35
Figure 4.3-8 Void fraction in the discharge tube @ L-CASE2.....4-36
Figure 4.3-9 Velocity in the vortex chamber @ S-CASE1.....4-37
Figure 4.3-10 Velocity in the vortex chamber @ S-CASE2.....4-38

Figure 4.3-11 Velocity vector in the discharge tube @ S-CASE1……4-39
Figure 4.3-12 Velocity vector in the discharge tube @ S-CASE2……4-40
Figure 4.3-13 Pressure distribution in the vortex chamber @ S-CASE1……4-41
Figure 4.3-14 Pressure distribution in the vortex chamber @ S-CASE2……4-42
Figure 4.3-15 Void fraction in the discharge tube @ S-CASE1……4-43
Figure 4.3-16 Void fraction in the discharge tube @ S-CASE2……4-44
Figure 4.3-17 Void Comparison between the test results and CFD evaluated results for differential pressure of the FD……4-45
Figure 4.3-18 Void Comparison between the test results and CFD evaluated results for K-factor……4-46
Figure 4.3-19 Comparison between the test results and CFD evaluated results for mass flow rate……..4-47

Acronyms and Abbreviations

BSL	Baseline
CFD	Computational Fluid Dynamics
DAS	Data Acquisition System
DVI	Direct Vessel Injection
ECCS	Emergency Core Cooling System
FD	Fluidic Device
KAERI	Korea Atomic Energy Research Institute
KHNP	Korea Hydro & Nuclear Power Co., Ltd.
LOCA	Loss of Coolant Accident
LPSIP	Low Pressure Safety Injection Pump
LT	Level Transmitter
PT	Pressure Transmitter
QOV	Quick Opening Valve
RMS	Root Mean Square
SIS	Safety Injection System
SIT	Safety Injection Tank
SST	Shear Stress Transport
VAPER	Valve Performance Evaluation Rig

1. INTRODUCTION

The SIT with FD (SIT-FD) is an accumulator tank that is partially filled with borated water and is pressurized with nitrogen. If the primary system pressure decreases below the nitrogen pressure of the SIT, water in the SIT is injected into the primary system through Direct Vessel Injection (DVI) nozzle by the differential pressure between the primary pressure and nitrogen pressure in the SIT. The FD is a passive flow controller, which is installed in the bottom of the SIT, which controls the discharge flow rate in a passive manner without any moving parts. The SIT-FD design has benefits for the reactor core cooling and the inherent reliability of safety system comparing with a conventional SIT design since FD can extend duration of the SIT operation by controlling the discharge flow during reflood phase of the Large Break Loss of Coolant Accident (LBLOCA). Adoption of the FD design allows an optimization of Emergency Core Cooling System (ECCS) in the APR1400 design by elimination of Low Pressure Safety Injection Pump (LPSIP) and reduces the core damage frequency of APR1400.

This Technical Report provides Computational Fluid Dynamics (CFD) analysis results of Fluidic Device (FD) in Safety Injection Tank (SIT). Topical Report [1] “Fluidic Device Design for the APR1400”, APR1400-Z-M-TR-12003-P, has been submitted to provide the operation mechanism, the performance of the SIT-FD and confirmatory full scale experiments. In the full scale experiments, however, detailed information in the vortex chamber and the discharge tube are not enough to understand the relationship between detailed flow characteristics in the vortex chamber and the performance of the SIT-FD, which may include cavitation phenomena.

The CFD analysis is specifically performed to demonstrate detailed flow characteristics in the FD under full scale experimental conditions and to confirm cavitation phenomena in the nozzle throat, using a CFD code.

2. OBJECTIVE

Based on the background in the Section 1, a series of CFD analysis is conducted to demonstrate the full scale experiment in terms of flow characteristics and cavitation phenomena in the SIT-FD, which could be strongly coupled with the performance of the SIT-FD. Expected results through the CFD analysis are described as below.

- Steady state calculation results of flow characteristics in the FD for both large and small flow mode and its impacts related to the performance of the FD
- Steady state calculation results of cavitation effects in the FD for both large and small flow mode and its impacts related to the performance of the FD
- Steady state calculation results of facing angle effects by comparing the performance of the nominal design with the performance of the maximum tolerance design due to a manufacturing tolerance.

3. ANALYSIS MODELS

3.1. SIT-FD Descriptions

Safety Injection System (SIS) is one of the subsystems of the ECCS in the APR1400 design. The SIS consists of four SIT-FD and four Safety Injection Pump (SIP), which are connected to the primary system via DVI nozzle. SIT is vertically mounted cylindrical tank and FD is a passive flow controller, which is installed in the bottom of the inner SIT. The SIT-FD contains borated water to a maximum of 2.5 weight percent boric acid and is pressurized with nitrogen to a nominal pressure of 4.21MPa(g) (610psig).

The FD has a supply port at the center and four control ports around the supply port with an equal circumferential angle of [ ]^{TS} at the surface top. The supply port is connected to a stand pipe that extends vertically.

The SIT water delivered through the supply port is divided into four directions with a relative angle of [ ]^{TS} by a partition plate, and then flows into the vortex chamber through four supply nozzles. On the other hand, the SIT water delivered through the four control ports flows directly into the vortex chamber through four control nozzles. Finally, the SIT water is discharged through an exit nozzle at the bottom center of the vortex chamber.

Control nozzles inject SIT water tangentially into the vortex chamber, establishing a strong swirling flow inside the vortex chamber when SIT water is only injected through the control nozzles. This causes a high flow resistance through the FD. In contrast to the control nozzle, each supply nozzle has an angle of [ ]^{TS} with a neighboring control nozzle. Consequently, the flow resistance through the FD is significantly decreased when SIT water is delivered into the vortex chamber through both the supply and control nozzles.

SIT water is delivered into the vortex chamber through both the supply and control nozzles at the early stage of LBLOCA when the SIT starts to operate and the stand pipe is covered with water. The SIT provides a large injection flow rate of SIT water which is required during the refill phase of LBLOCA. When the SIT water level is lowered to below the top of the stand pipe, the flow path via the supply nozzle is terminated and all SIT water is delivered only through the control nozzle. As a result, the injection flow rate of the SIT water is decreased, but is still sufficient to remove decay heat during the reflood phase, extending the total duration of the SIT water injection.

3.2. Geometrical Modeling and Mesh Configuration

Two separate CFD models are generated for two different flow characteristics in large flow and small flow mode in order to apply the two different boundary conditions of the CFD models in each injection mode. The SI water flows into both supply ports and control ports in the large flow mode but the SI flow from the supply ports is terminated in the small flow mode. Therefore, a common one model for simulating both the large and the small flow mode is not applicable for this analysis.

Geometrical modeling and mesh configuration methods are described as follow.

3.2.1 Geometrical Modeling

Figure 3.2-1 and Figure 3.2-2 shows the geometrical models for each injection mode.

3.2.1.1 Large Flow Mode

a. The SIT is modeled from top of the FD to the water free surface level which remains stationary in all large flow cases.

   (Note1) Water free surface level is determined as [ ]^{TS} obtained from the level transmitter (LT)-101. This value is measured at 16.89 second in Test Case-01-01, which is corresponded with L-CASE1 in the CFD analysis (See Table 4.1-1).

b. The configuration of FD is precisely modeled such as partition plate, closure plate, vortex chamber, insert plate and lower plate.

c. The exit nozzle and discharge tube are precisely modeled.

d. The first elbow in the discharge pipe line is precisely modeled.

e. The discharge pipe line in the experiment is partially modeled to the location of the pressure transmitter (PT) which is installed in the discharge pipe line (PT-102, see Ref 1. Fig. 4.1-1).

3.2.1.2 Small Flow Mode

a. The SIT is modeled from top of the FD to the top of the standpipe. The water level remains stationary in all small flow cases.

   (Note1) Water free surface level is same with the level of the standpipe.

b. The configuration of FD is precisely modeled such as partition plate, closure plate, vortex chamber, insert plate and lower plate.

c. The exit nozzle and discharge tube are precisely modeled.

d. The first elbow in the experiment is precisely modeled.

e. The discharge pipe line in the experiment is partially modeled to the location of the pressure transmitter which is installed in the discharge pipe line (PT-102, see Ref 1. Fig. 4.1-1)

(a) Model for large flow mode

(b) Model for small flow mode

Figure 3.2-1 Geometrical models for CFD analysis (Side-view)

Figure 3.2-2 Geometrical models for CFD analysis (Bottom-view)

3.2.2 Mesh Configuration

Mesh generation was conducted using ANSYS ICEM CFD Version 14.5. Basically, mesh configuration strategy for both large and small flow mode is to use a tetrahedron mesh (Unstructured mesh) for the SIT and FD inner volume due to the complex design of the FD and a prism mesh (Structured mesh) for resolving the boundary layer.

The flow of inner SIT for both large and small flow mode has an insignificant effect on the cavitation phenomena and the performance of the FD. On the other hand, the vortex chamber, the exit nozzle and the discharge tube has steep velocity and pressure gradients in both large and small flow mode hence a finer mesh is generated in these regions. Figure 3.2-3 and Figure 3.2-4 show the mesh configurations in the side-view and the bottom-view. Figure 3.2-5 shows the prism layers for resolving the boundary layer. The difference of the mesh configuration between the large flow mode and small flow is only the number of the SIT volume mesh above the standpipe level.

Based on the preliminary calculation, the first layer thickness had been determined as [ ]TS to make Y+ value less than 300 in both large flow and small flow mode using a prism mesh type. Total number of the prism layer was set by [ ]TS and the growth ratio of the prism mesh is set by [ ]TS. Table 3.2-1 represents the total number of elements for each injection mode and observed maximum Y+ value and observed the location of maximum Y+ value (See Figure 3.2-6 and 3.2-7).

In the mesh sensitivity analysis (See Section 4.2.2), the mesh refinement is conducted by three steps such as coarse, medium, fine. Through the pre-calculation, the mesh generation at fine level is fixed to simulate the proper phenomena in the SIT-FD then the mesh generation at coarse level and medium level are performed by adjusting the global scale factor of the element, which is provided by ANSYS ICEM-CFD software. The first layer thickness, the number of the prism layer and the growth ratio of the prism are also same with above. Table 3.2-2 shows the results of the mesh refinement at three levels.

Table 3.2-1 Total number of elements for the large flow and small flow mode TS

Table 3.2-2 Mesh refinement information for the mesh sensitivity analysis TS

(a) Mesh configuration for large flow mode

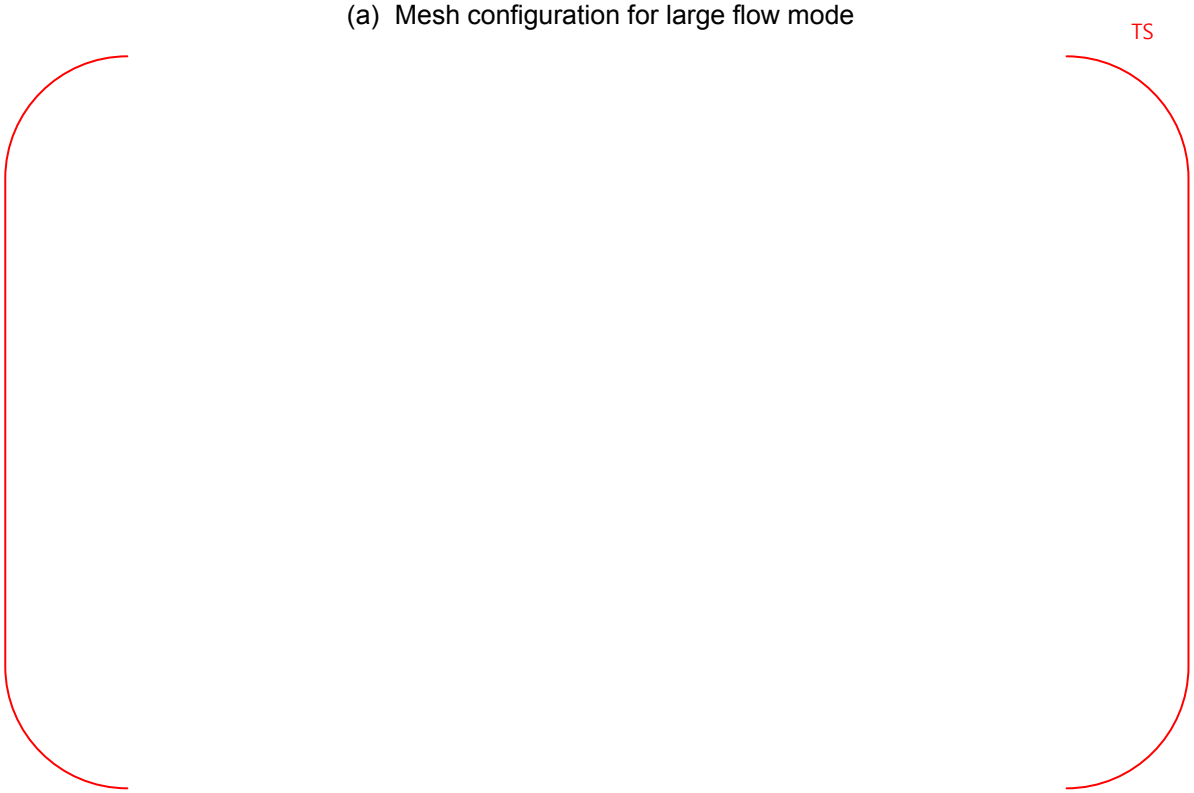

(b) Mesh configuration for small flow mode

Figure 3.2-3 Mesh configuration (Side-view)

TS

(a) Mesh configuration for large flow mode

TS

(b) Mesh configuration for large flow mode

Figure 3.2-4 Mesh configuration (Bottom-view)

Figure 3.2-5 Prism mesh for boundary layer

TS

Figure 3.2-6 Maximum Y+ for large flow case

TS

Figure 3.2-7 Maximum Y+ for small flow case

3.3. Numerical Models

In this section, governing equations, numerical models and correlation factors, which are used in this CFD analysis, are summarized as follow. (See Ref. 2)

3.3.1 Time dependence

Steady-state calculation for both injection modes.

3.3.2 Multiphase flow model

TS

3.3.3 Type of fluids

TS

3.3.4 Governing equations

TS

TS

3.3.5 Turbulence model

Shear Stress Transport (SST) model.

SST model is started from the $k-\omega$ model and the Baseline (BSL) $k-\omega$ model.

$$\frac{\partial(\rho k)}{\partial t}+\frac{\partial(\rho U_j k)}{\partial x_j}=\frac{\partial}{\partial x_j}\left[\left(\mu+\frac{\mu_t}{\sigma_{k3}}\right)\frac{\partial k}{\partial x_j}\right]+P_k-\beta'\rho k\omega+P_{kb}$$

$$\frac{\partial(\rho\omega)}{\partial t}+\frac{\partial(\rho U_j\omega)}{\partial x_j}=$$

$$\frac{\partial}{\partial x_j}\left[\left(\mu+\frac{\mu_t}{\sigma_{\omega 3}}\right)\frac{\partial\omega}{\partial x_j}\right]+\alpha_3\frac{\omega}{k}P_k-\beta_3\rho\omega^2+P_{\omega b}+(1-F_1)2\rho\frac{1}{\sigma_{\omega 2}\omega}\frac{\partial k}{\partial x_j}\frac{\partial\omega}{\partial x_j}$$

Where, all coefficients are shown as follow.

TS

Undefined coefficients expressed lowercase letters 3 are a linear combination of the corresponding of the above coefficient.

$$\emptyset_3 = F_1\emptyset_1 + (1 - F_1)\emptyset_2$$

The BSL model has the advantages of the Wilcox model and the $k-\varepsilon$ model, but still fails to predict the onset and amount of flow separation. Mentor suggested the proper transport behavior using a limiter to the formulation of the eddy-viscosity.

$$\nu_t = \frac{a_1 k}{\max(a_1 k, SF_2)}$$

Where, ν is kinematic viscosity.

$$\nu_t = \frac{\mu_t}{\rho}$$

F_1 and F_2 are blending functions as underlying expressions, S is an invariant measure of the strain rate.

The blending functions, F_1

$$F_1 = \tanh\left[\left(\min\left(\max\left(\frac{\sqrt{k}}{\beta'\omega y}, \frac{500\nu}{\omega y^2}\right), \frac{4\rho k}{CD_{k\omega}\sigma_{\omega 2} y^2}\right)\right)^4\right]$$

Where, y is the distance to the nearest wall and

$$CD_{k\omega} = \max\left(2\rho\frac{1}{\sigma_{\omega 2}\omega}\frac{\partial k}{\partial x_j}\frac{\partial \omega}{\partial x_j}, 1.0\times 10^{-10}\right)$$

The blending functions, F_2

$$F_2 = \tanh\left[\left(\max\left(\frac{2\sqrt{k}}{\beta'\omega y}, \frac{500\nu}{\omega y^2}\right)\right)^2\right]$$

3.3.6 Near wall treatment

In ANSYS CFX software, automatic near-wall treatment is activated automatically when SST model is used. Automatic near-wall treatment automatically switches from wall-function to a low-Reynolds near wall formulation as the mesh is refined. Generally, Y+, which is the non-dimensional distance from the wall, should be lower than 300 for the wall function. To use a strict low-Reynolds number formulation, a near wall mesh resolution should be lower than 2. In this technical report, the maximum Y+ values in the fluid domain at all analysis cases are set under 300. (See Section 3.2.2)

3.3.7 Cavitation model

Rayleigh-Plesset Model

$$\dot{m}_{fg} = F\frac{3r_{nuc}(1-r_g)\rho_g}{R_{nuc}}\sqrt{\frac{2}{3}\frac{|p_v-p|}{\rho_f}}\,sgn(p_v-p)$$

Where, F is an empirical factor, F_{vap} is an empirical factor for vaporization, F_{cond} is an empirical factor for condensation, R_{nuc} is nucleation site radius, r_{nuc} is the volume fraction of the nucleation sites, p_v is the vapor pressure for the liquid, p is a reference pressure for the flow.

In cavitation model, above factors are set as below. TS

[ ]

3.3.8 Advection scheme

In this technical report, the advection scheme sensitivity analysis for selecting the advection scheme is performed as described in the section 4.2.1.

3.3.9 Other

Pressurized nitrogen in the top of SIT and evolution of dissolved nitrogen gas are not modeled.

3.3.10 Convergence Criteria

The residual is the local imbalance of each control volume equations. The root mean square (RMS) normalized residuals is selected to check the local imbalance for convergence.

- Criteria : All RMS residuals have to be below [ ] TS

The global imbalance is defined as below.

$$\text{Global imbalance}(\%\text{ imbalance}) = \frac{\text{Domain imbalance}}{\text{Maximum imbalance over all domains}}$$

- Criteria: Global imbalance has to be below [ ]TS

4. CFD ANALYSIS

4.1. Boundary Conditions and Analysis Matrix

The main driven force of the SIT-FD is the differential pressure between nitrogen pressure and outlet pressure and the hydraulic head by the SIT water level partially contributes to driven force. Based on a preliminary analysis, the combination of a pressure inlet and outlet boundary condition often showed the numerical instability and the non-physical solutions or failure of the solution to converge due to the imbalance of mass and momentum. ANSYS CFX software recommends that the inlet and outlet boundary conditions are set as the velocity or mass flow rate at an inlet and pressure at an outlet.

a. Large flow mode
   - Inlet boundary condition: Measured flow rate
   - Location of the inlet boundary condition: Top surface of the SIT
   - Outlet boundary condition: Measured gauge pressure (PT-102)
   - Location of the outlet boundary condition: End surface of the discharge pipe line

b. Small flow mode
   - Inlet boundary condition: Measure flow rate
   - Location of the inlet boundary condition: Top surface of the SIT except for the top surface of the standpipe
   - Outlet boundary condition: Measured gauge pressure (PT-102)
   - Location of the outlet boundary condition: End surface of the discharge pipe line

The measured flow rate in both large and small flow mode have an oscillation due to the measurement uncertainty of the level transmitter. Before the selecting of the boundary condition in large and small flow mode, the linear data fitting of the measured flow rate is performed at the Test Case-01-01.

The measured data are selected for the boundary condition in accordance with a following qualitative judgment.

The full scale experiment begins by opening the quick opening valve (QOV). The opening time of QOV is estimated about [ ]^{TS} seconds. In this period, the opening characteristic of QOV, which means pressure drop of valve, is continuously changed. To avoid the hysteresis effect of the valve opening, the measured data for the boundary conditions are selected in large flow mode after the QOV is fully opened. Since flow rate of the SIT-FD is turning down from large to small at around [ ]^{TS} seconds, the period of large flow mode can be defined from [ ]^{TS} seconds to [ ]^{TS} seconds. In CFD calculation, total 3 points are selected for the analysis matrix during the large flow mode.

At around [ ]TS second, turning down of the flow begins from large to small and duration of the turning down is about [ ]TS seconds. The Topical Report of SIT-FD states that the air in the top of the SIT started to be discharged through the empty standpipe at [ ]TS seconds. In this technical report, CFD analysis methodology is focused on the cavitation effect and its related to the performance of SIT-FD thus the air discharge phenomena is not considered.

Therefore the period of small flow mode can be defined from [ ]TS seconds to [ ]TS seconds. Total 5 points are selected for analysis matrix during the small flow mode. Analysis matrix, detailed boundary conditions and time points are summarized as shown in Table 4.1-1.

Table 4.1-1 Summary of boundary conditions for large and small flow mode TS

Figure 4.1-1 Linear fitting data and CFD analysis points for large flow and small flow mode (Test Case-01-01)

4.2. Sensitivity Analysis

4.2.1 Advection Scheme Sensitivity

In this section, a sensitivity analysis is performed to determine the advection scheme for simulating the flow characteristics in the vortex chamber, which has a steep spatial gradient during whole discharge period of the SIT-FD.

In the large and small flow mode, a highly steep velocity and pressure gradient occurs in the vortex chamber and exit nozzle thus the advection scheme can affect the pressure loss characteristics and the flow structures in the nozzle throat. The cavitation phenomena depends on the minimum pressure at the nozzle throat and the intensity of swirling flow, and therefore an advection scheme should be selected for simulating a proper phenomena in the SIT-FD.

4.2.1.1 Advection Schemes

In ANSYS CFX software, several different schemes are provided to approximate the value of advection term at the integration point of a control volume.

The advection term can be cast as follow.

$$\varphi_{ip} = \varphi_{up} + \beta \nabla\varphi \cdot \Delta\vec{r}$$

Where, φ_{ip} is the value at the integration point, φ_{up} is the value at the upwind node, $\vec{r}$ is the vector from the upwind node to the ip, Particular choices for β and $\nabla\varphi$ provide different schemes such as Upwind, Specified Blend and High resolution scheme.

$\beta = 0$ means the 1st order upwind scheme.

The quantity $\beta \nabla\varphi \cdot \Delta\vec{r}$, called the numerical advection correction, can be adjusted by choosing a value for β between 0 and 1 and it is called Specified Blend Scheme.

The High Resolution scheme uses a special nonlinear recipe for β at each node, computed to be as close to 1 as possible. The recipe for β involves first computing a φ_{min} and φ_{max} at each node and then above equation is solved for β to ensure that it does not undershoot φ_{min} and overshoot φ_{max}.

4.2.1.2 Boundary conditions and Test Matrix

The advection scheme sensitivity analysis is performed using the boundary conditions of L-CASE1 and S-CASE2 (See Section 4.1.1), which represents for the large flow and the small flow mode. Table 4.2-1 shows the test matrix for advection scheme sensitivity.

4.2.1.3 Results

The pressure loss coefficient (K-factor) of the FD is evaluated by comparing the mean value of the measured data in the Test Case-01-01 with the CFD results. The CFD evaluated K-factors in each advection scheme are given in Table 4.2-2, Figure 4.2-1 and 4.2-2.

The CFD evaluated K-factor reaches at the experimental data when the blend factor is [ ]^{TS}. The Upwind scheme, which means the first order scheme, under-predicts the K-factor less than the experiment data and the other schemes because the Upwind scheme neglects the adjacent nodal gradient $\nabla\varphi$ in the region of the nozzle throat. The CFD evaluated K-factor is closed to the mean value of the test results when β is increased. As shown from Figure 4.2-3 to Figure 4.2-5, the [ ]^{TS} case shows that the volume of the vaporous cavitation is larger than the upwind case, and hence the CFD evaluated K-factor in the [ ]^{TS} is larger than the upwind case.

However, the higher β cases of the Specified Blend schemes and the High resolution scheme have not converged solutions as given in Table 4.2-2. ANSYS CFX user manual states that the second order High Resolution advection scheme has the desirable property of giving 2nd order accurate gradient resolution, but may cause convergence problems due to the nonlinearity of the β value. In addition, the Specified Blend scheme in case that β is closed to 1 may introduce dispersive discretization errors that tend to cause non-physical oscillations in regions of rapid spatial gradient.

In conclusion, the blend factor β is selected as [ ]^{TS} for simulating flow characteristics in the SIT-FD.

Table 4.2-1 Test Matrix for the advection scheme sensitivity

TS

Table 4.2-2 Analysis results for the advection scheme sensitivity

TS

Figure 4.2-1 Results of sensitivity analysis for selecting the advection scheme
(Large flow mode, L-CASE1)

Figure 4.2-2 Results of sensitivity analysis for selecting the advection scheme
(Small flow mode, S-CASE2)

Figure 4.2-3 Void fraction in the exit nozzle @ Upwind case

TS

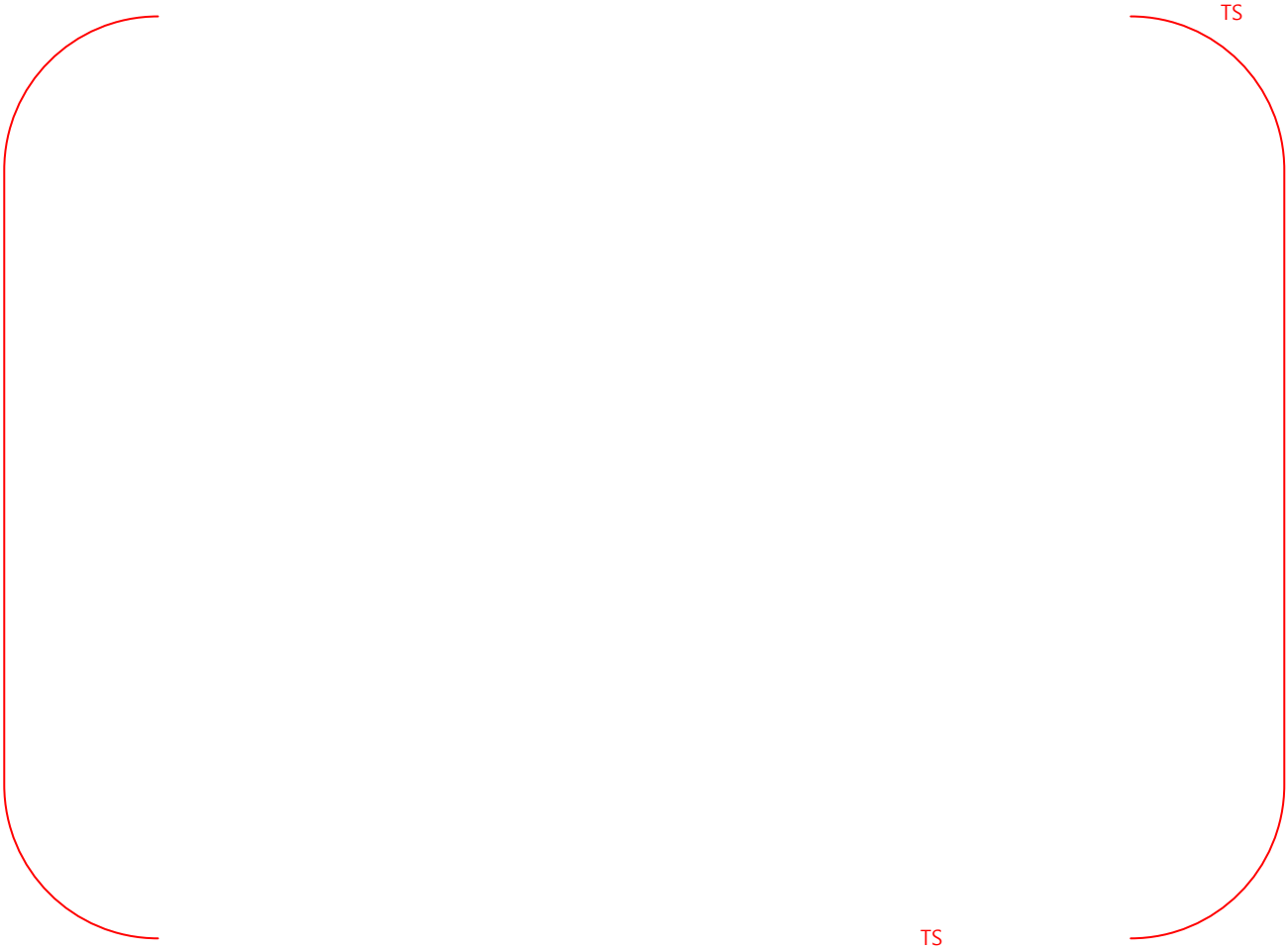

Figure 4.2-4 Void fraction in the exit nozzle @ SB-[ ]TS case

TS

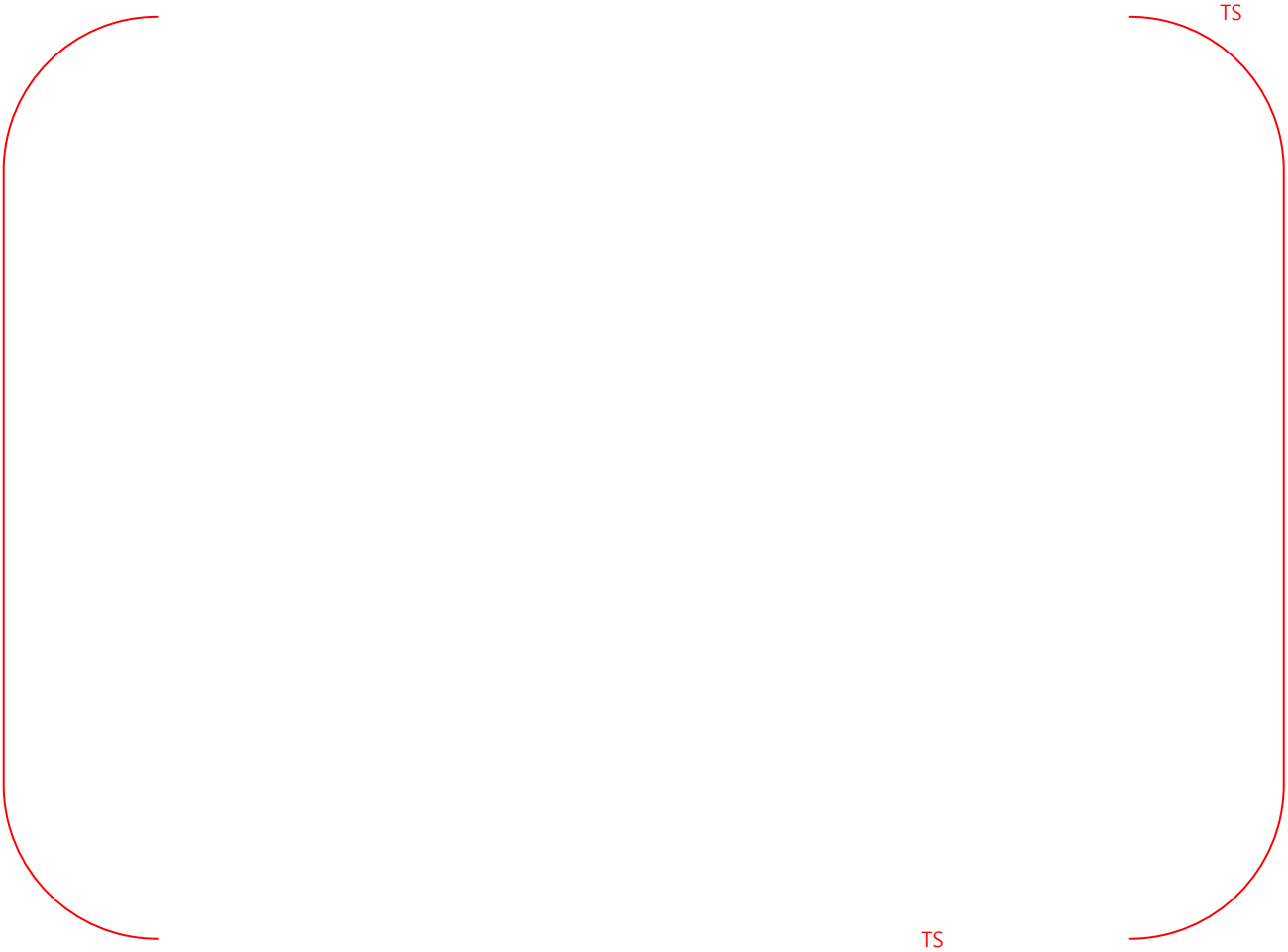

Figure 4.2-5 Void fraction in the exit nozzle @ SB-[TS] case

4.2.2 Mesh Sensitivity Analysis

The discretization error of CFD analysis should be thoroughly checked by conducting the mesh refinement analysis. In this section, the results of mesh sensitivity analysis are described using three different mesh configurations.

4.2.2.1 Geometrical Model and Mesh Configuration

The geometrical model for small flow mode is used in this sensitivity analysis. Detail mesh configuration method is described in Section 3.2.2.

4.2.2.2 Boundary Conditions

The boundary condition of S-CASE2 is used (See Table 4.1.1)

In order to calculate the advection term, a Specified Blend scheme is used in this sensitivity analysis and the blend factor is set by [ ]^{TS} (See Section 4.2.1)

4.2.2.3 Results

Table 4.2-3 and Figure 4.2-6 show the results of the mesh sensitivity analysis.

In case of the coarse mesh configuration, the CFD evaluated K-factor largely deviate from the mean value of the test data. The CFD evaluated K-factor shows an asymptotic convergence as grid is refined, and is within the uncertainty range of the test results in a fine level.

Based on this mesh refinement analysis, mesh configuration is determined as a fine level.

Table 4.2-3 Analysis results for the mesh sensitivity analysis

TS

Figure 4.2-6 Results of mesh sensitivity analysis

4.2.3 Manufacturing Tolerance of Facing Angle Sensitivity

In large flow mode, the SI water flows through both the supply and control port simultaneously. Each supply nozzle has an angle of [ ]TS with neighboring control nozzles in the vortex chamber. In this case, the two opposite directions of flows are merged with each other inside the vortex chamber and the merged flow is directly discharged toward the center of the nozzle throat.

In the manufacturing stage, this facing angle can be distorted from the nominal design to the maximum tolerance design due to the manufacturing tolerance thus the flow structure in the vortex chamber may be affected by the distorted facing angle, can change the performance of the SIT-FD in each injection mode.

In this section, facing angle sensitivity analysis is performed in both large and small flow mode.

4.2.3.1 Geometrical Model and Mesh Configuration

The manufacturing tolerance of the facing angle is [ ]TS, which is provided by the manufacturer. In this sensitivity analysis, distorted facing angle is set by [ ]TS to cover the manufacturing tolerance.

Figure 4.2-7 shows the three different of geometrical models for facing angle sensitivity analysis.

- Model 1: Facing angle is [ ]TS.
- Model 2: Facing angle is [ ]TS. (Basecase)
- Model 3: Facing angle is [ ]TS.

The other design parameters are same with the nominal design as described in the section 3.2.1.

Mesh generation methodology is also same with the section 3.2.2.

Table 4.2-4 shows the results of the mesh generation for the facing angle sensitivity analysis.

4.2.3.2 Boundary Conditions

The facing angle sensitivity analysis is conducted using the boundary conditions of L-CASE1 and S-CASE2 as described in the section 4.1.1.

4.2.3.3 Results

Table 4.2-5 shows the results for facing angle sensitivity analysis.

In large flow mode, the maximum difference of CFD evaluated K-factor between the maximum tolerance design and the nominal design is [ ]TS in L1 case. In small flow mode, the maximum difference of K-factor between the maximum tolerance design and the nominal design is [ ]TS. As described in the TR of the SIT-FD, The total uncertainty of K-factor is [ ]TS in the large flow mode, and is [ ]TS in the small flow mode. The CFD evaluated K-factors in small flow mode

are within the uncertainty ranges of the test results but the K-factors in large flow mode deviate from the uncertainty ranges.

Meanwhile, the design requirement ranges of the K-factor from the SIT-FD to DVI nozzle are;

[- TS
-]

Since the range of the K-factor of the expected SI line from the SIT-FD nozzle to the DVI nozzle is [ ]TS hence the design requirement ranges of the FD K-factor are;

[- TS
-]

Using these ranges of K-factor above, LBLOCA calculation is performed (Ref. 3) and the results have enough margins to meet the acceptance criteria.

In conclusion, the facing angle effect originated from the manufacturing tolerance has an insignificant effect on the performance of the SIT-FD.

Table 4.2-4 Total number of elements and Test Matrix for the facing angle sensitivity analysis

TS

TS

Table 4.2-5 Analysis results for the facing angle sensitivity analysis

Figure 4.2-7 Comparison of the geometry model for the facing angle sensitivity analysis

TS

Figure 4.2-8 Void fraction in the exit nozzle @ L1 case

Figure 4.2-9 Void fraction in the exit nozzle @ L3 case

Figure 4.2-10 Void fraction in the exit nozzle @ S1 case

Figure 4.2-11 Void fraction in the exit nozzle @ S3 case

4.3. Analysis Results

4.3.1 Large flow mode

Detailed flow structures are shown in Figure 4.3-1 to Figure 4.3-2. In large flow mode, the SIT water delivered through both supply ports and control ports. The SI flow from the control nozzle and the supply nozzle merges with each other due to the facing angle design and the main streams of the merged flow discharges toward the center of the nozzle throat. Near the exit nozzle, four main streams develop a core vortex, which is not strong vortex. Figure 4.3-3 and 4.3-4 illustrates the velocity vector in the exit nozzle and the discharge tube. The velocity of the nozzle throat is accelerated to [ ]^{TS}. Due to this, the local pressure at the center of the nozzle throat and the discharge tube reached at the saturation pressure of [ ]^{TS} as shown in Figure 4.3-5 and 4.3-6.

Figure 4.3-7 and 4.3-8 shows the formation of vaporous cavitation at the center region of the discharge tube. However, there is no flow blockage in the discharge tube and the SI water flows through a narrow gap between the wall of the discharge tube and the vaporous cavitation. Near the end of the diffuser, the local pressure is recovered due to diffuser effect and a viscous effect of a wall boundary layer, and thus recirculation flow is generated in this region.

The CFD evaluated K-factors in the large flow mode are under-predicted comparing with the uncertainty range of the test. The maximum deviation from the mean value of the test is [ ]^{TS} in the L-CASE3. However, the CFD evaluated K-factors in large flow mode are acceptable considering the design requirement range of the SIT-FD as discussed in Section 4.2.3.3.

4.3.2 Small flow mode

In small flow mode, the SIT water delivered through only control ports. Due to the design of the control nozzle, a highly swirling flow occurs in the vortex chamber. Detailed flow structures are illustrated from Figure 4.3-9 to Figure 4.3-16.

As shown in Figure 4.3-9 and 4.3-10, the flow through the control nozzles is delivered tangentially into the vortex chamber and flows out to the exit nozzle with a strong vortex flow in the vortex chamber. CFD analysis shows the detailed flow characteristics in the small flow period as expected design concept of the SIT-FD.

When the strong vortex flow passes through the nozzle throat, the local pressure near the wall of nozzle throat is relatively increased and the local pressure near the center of the vortex core is decreased due to a centrifugal force. Because of this, the local pressure at the center of the vortex core is decreased at the saturation pressure of [ ]^{TS} water and the vaporous cavitation is formed in the center of the exit nozzle throat. Therefore the SIT water flows into the narrow gap between the exit nozzle wall and the vaporous cavitation as shown in Figure 4.3-15 and 4.3-16. When the flow is delivered into the narrow gap, the velocity is accelerated about [ ]^{TS}. After the flow passes the narrow gap, the centrifugal force and the fluid velocity is decreased due to a viscous effect of a wall boundary layer, and then flow recirculation occurs along the centerline of the discharge tube, which allows the reverse flow as shown in Figure 4.3-11 and 4.3-12.

The CFD evaluated K-factors are predicted within the fluctuation range of the experiment result as shown in Figure 4.3-19. But the CFD evaluated K-factors of S-CASE3, S-CASE4 and S-CASE5 deviate from the uncertainty ranges of the test data. In these cases, the blend factor for the advection term is used as [ ]^{TS}. After the blend factor is used as [ ]^{TS}, the K-factor becomes smaller than the [ ]^{TS} cases. During whole discharge period of the SIT-FD, flow velocity and pressure drop are gradually decreased thus we expect that the specified blend factor can be changed in accordance with a specific flow rate condition. Consequently, the results of these 3 cases such as the CFD evaluated K-factor and the vaporous caviation are more conservative than the mean value of the test data.

Table 4.3-1 Analysis results for the large flow and small flow mode

TS

TS

Figure 4.3-1 Velocity in the vortex chamber @ L-CASE1

TS

Figure 4.3-2 Velocity in the vortex chamber @ L-CASE2

Figure 4.3-3 Velocity vector in the discharge tube @ L-CASE1

Figure 4.3-4 Velocity vector in the discharge tube @ L-CASE2

Figure 4.3-5 Pressure distribution in the vortex chamber @ L-CASE1

TS

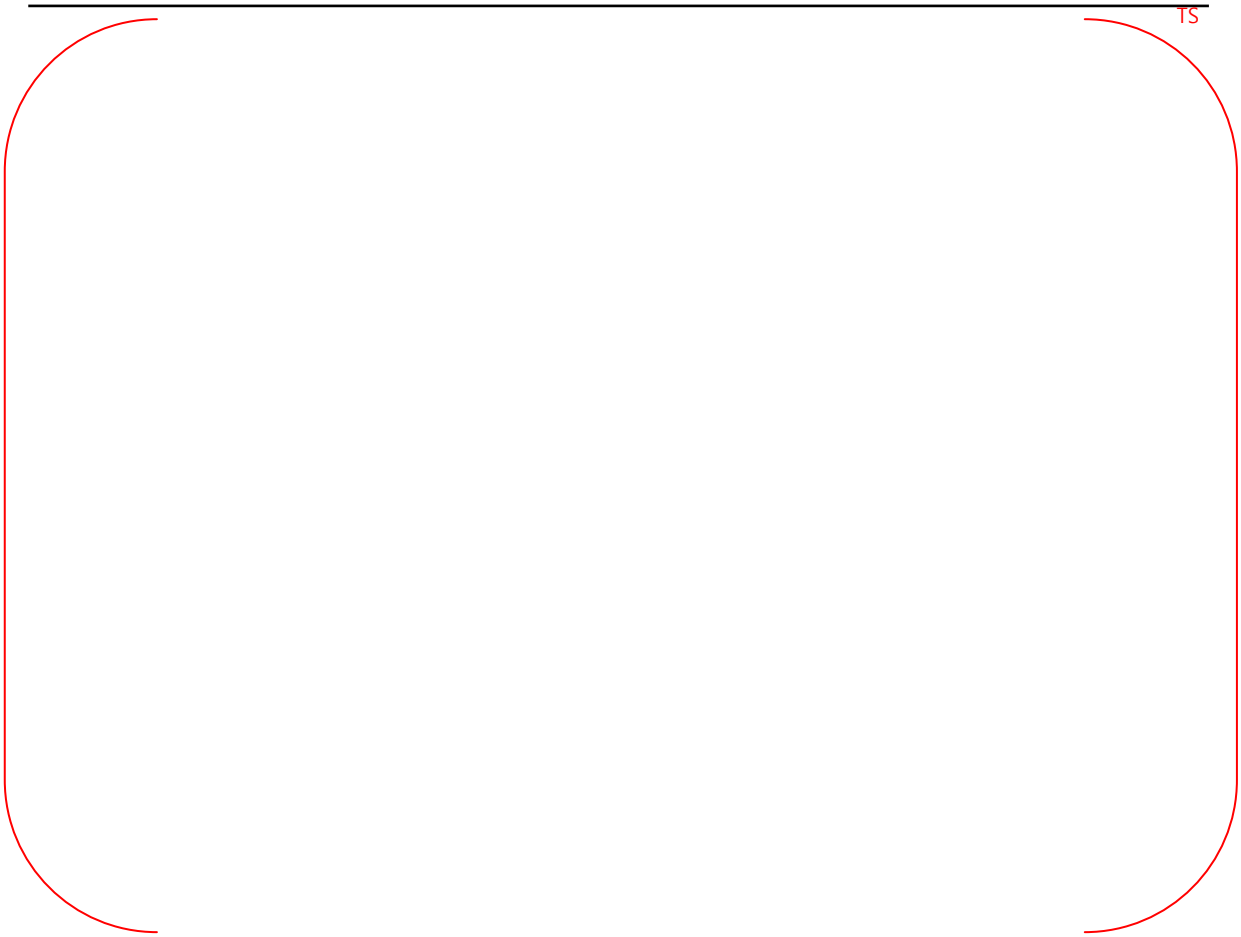

Figure 4.3-6 Pressure distribution in the vortex chamber @ L-CASE2

TS

Figure 4.3-7 Void fraction in the discharge tube @ L-CASE1

Figure 4.3-8 Void fraction in the discharge tube @ L-CASE2

TS

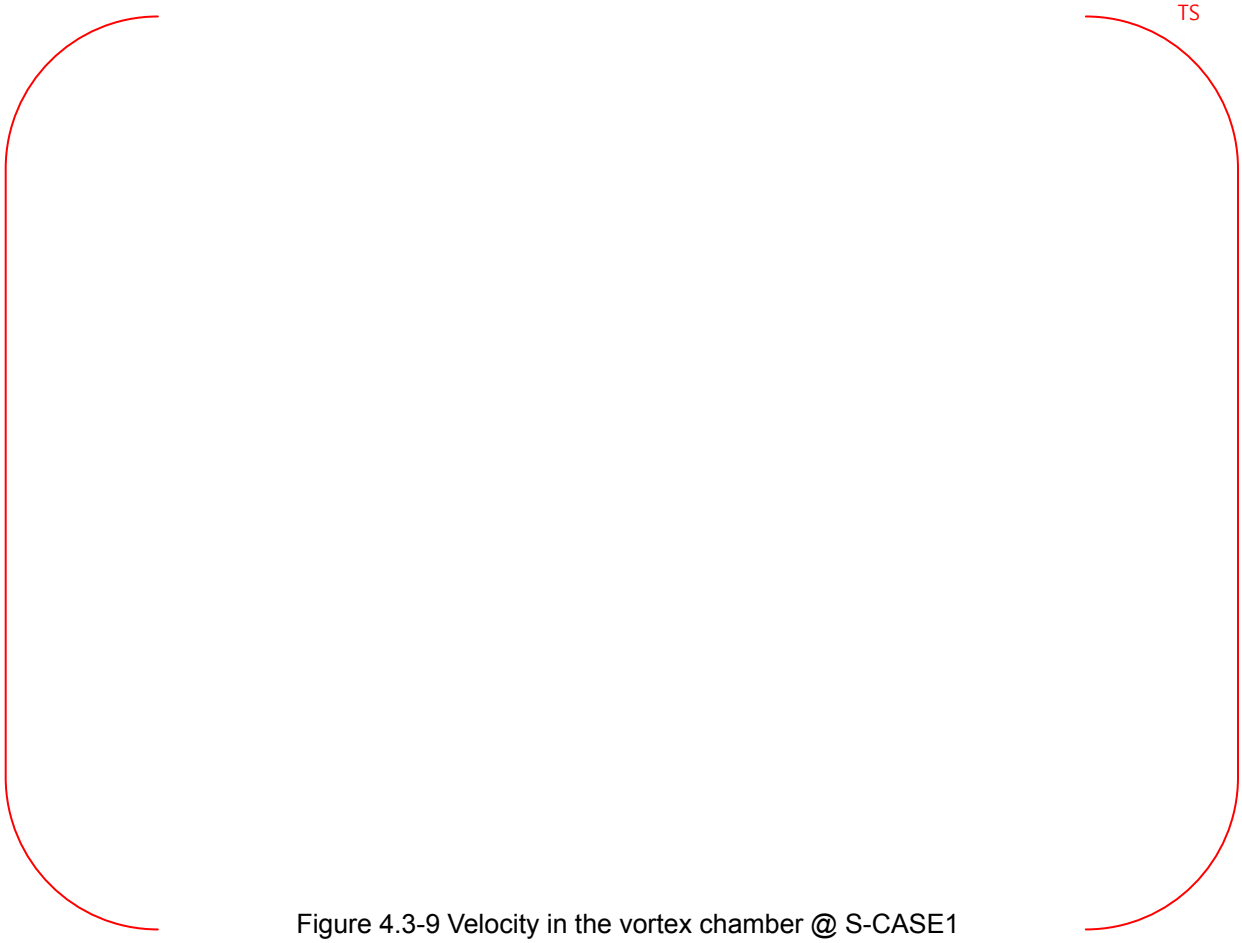

Figure 4.3-9 Velocity in the vortex chamber @ S-CASE1

Figure 4.3-10 Velocity in the vortex chamber @ S-CASE2

Figure 4.3-11 Velocity vector in the vortex chamber @ S-CASE1

Figure 4.3-12 Velocity vector in the vortex chamber @ S-CASE2

Figure 4.3-13 Pressure distribution in the discharge tube @ S-CASE1

Figure 4.3-14 Pressure distribution in the discharge tube @ S-CASE2

Figure 4.3-15 Void fraction in the discharge tube @ S-CASE1

Figure 4.3-16 Void fraction in the discharge tube @ S-CASE2

Figure 4.3-17 Comparison between the test results and CFD evaluated results for differential pressure of the FD

Figure 4.3-18 Comparison between the test results and CFD evaluated results for K-factor

Figure 4.3-19 Comparison between the test results and CFD evaluated results for mass flow rate

5. CONCLUSION

Topical Report “Fluidic Device Design for the APR1400” provides the working principles of the flow controlling the FD, the performance of the SIT-FD based on the confirmatory full scale experiments. The results show that the performance of the SIT-FD satisfies the design requirements and the reproducibility of the performance is confirmed. However, the results of the full scale experiment provide insufficient informations for detail flow structure in the vortex chamber, occurrence of cavitation phenomena and the performance of maximum tolerance design due to manufacturing tolerances.

This technical report provides the results of analysis for the demonstration of the detail flow structure of the SIT-FD, the performance of the SIT-FD and the maximum tolerance design effects with a cavitation modeling using ANSYS CFX code. Conclusions of the CFD analysis results are summarized as below.

- The CFD analysis shows that the detailed flow structure of the vortex chamber in both large flow and small flow mode are satisfied with the intended design concept of the SIT-FD.
- The CFD evaluated K-factors of the large and the small flow mode in the maximum tolerance design are within the uncertainty ranges or the design requirement rages. Therefore, the performance of the SIT-FD is not affected by the maximum tolerance facing angle due to the manufacturing tolerance.
- Vaporous cavitation can occurs in the nozzle throat and the discharge tube in both large flow and small flow mode but there was no effect of the pressure loss in the FD by a flow blockage due to the vaporous cavitation.
- The impacts of cavitation on SIT flow rates and FD K-factors are directly addressed by the results of the full scale experiment.

6. REFERENCES

[1] APR1400-Z-M-TR-12003-P, Rev. 0, “Fluidic Device Design for the APR1400”, December, 2012.

[2] ANSYS CFX 14.5 Documentation, “Theory Guide”, November, 2011.

[3] APR1400-F-A-TR-12004-P, Rev. 0, “CAREM, LBLOCA Analysis Methodology”, December, 2012.